Numerical simulation of infrasound propagation in the Earth's atmosphere: Study of a stratospherical arrival pair

R. Sabatini, O. Marsden, C. Bailly, and O. Gainville

Citation: AIP Conference Proceedings **1685**, 090002 (2015); doi: 10.1063/1.4934468
View online: http://dx.doi.org/10.1063/1.4934468
View Table of Contents: http://scitation.aip.org/content/aip/proceeding/aipcp/1685?ver=pdfcov
Published by the AIP Publishing

Numerical Simulation of Infrasound Propagation in the Earth's Atmosphere: Study of a Stratospherical Arrival Pair

R. Sabatini[1,2,a)], O. Marsden[1], C. Bailly[1] and O. Gainville[2]

[1]*LMFA, UMR CNRS 5509 & École Centrale de Lyon, 69134 Écully cedex, France.*
[2]*CEA, DAM, DIF, F-91297 Arpajon, France.*

[a)]Corresponding author: roberto.sabatini@doctorant.ec-lyon.fr

Abstract. A direct numerical simulation of the two-dimensional unsteady compressible Navier-Stokes equations is performed in order to compute the sound field generated by a high-amplitude infrasonic source in a realistic stratified atmosphere and in the presence of a stratospheric wind. Nonlinear distortion as well as wind convection effects on the stratospheric arrivals recorded at ground level are investigated and discussed. Finally, a comparison with infrasonic signals collected from the vapour cloud explosion which occurred at Buncefield, UK, in 2005, is also carried out.

INTRODUCTION

Infrasonic waves propagate in the Earth's atmosphere along cyclic trajectories induced by the speed of sound and wind gradients, and can be recorded at distances of hundreds to thousands of kilometres from their source [1]. They are typically refracted upward in the troposphere, due to the decrease of the temperature, and then refracted back towards the ground at stratospheric and thermospheric altitudes. Stratospheric arrivals are generally detected in the direction of wind jets. Furthermore, they can arrive in pairs and at very high celerities (Figure 1(a)), the celerity being defined as the quotient between the distance source-recording station and the travel time [2]. A spectacular manifestation

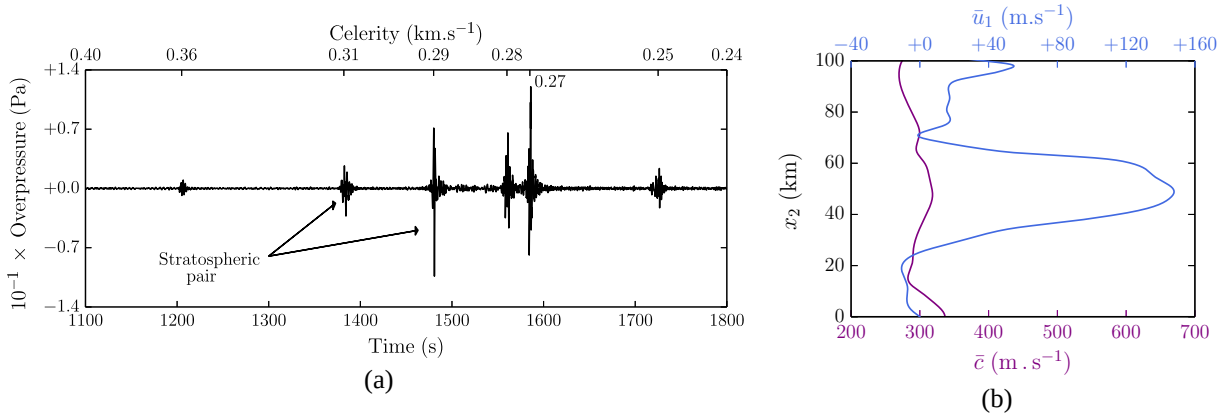

FIGURE 1. (a) Overpressure p' recorded at the ground station DIA, located in the Netherlands at 435 km from Buncefield. (b) Speed of sound $\bar{c}$ and horizontal wind $\bar{u}_1$ profiles.

of this phenomenon was observed just after the large vapour cloud explosion which occurred at the Buncefield Oil Depot, United Kingdom, in 2005 [2, 3, 4]. Fast stratospheric signals with frequencies in the range [0.1 Hz, 1 Hz] were detected in the Netherlands with celerities even greater than the speed of sound at ground level. These fast arrivals were induced by a strong wind propagating eastwards with a velocity of almost 150 m.s^{-1} at about 50 km altitude.

Recent Developments in Nonlinear Acoustics
AIP Conf. Proc. 1685, 090002-1–090002-4; doi: 10.1063/1.4934468

In the present work, a simulation of the two-dimensional unsteady compressible Navier-Stokes equations is performed to analyse the propagation of a high-amplitude infrasonic signal in a realistic stratified atmosphere constructed from the speed of sound and horizontal wind profiles measured between the Buncefield source location and the DIA infrasound array (Netherlands). A high-order finite-difference time-domain method originally developed for aeroacoustic applications is employed for the computations. Nonlinear distortion and wind effects on the stratospheric arrivals recorded at ground level are investigated. A comparison between the numerical results and the infrasonic signal detected at DIA is also presented.

PROBLEM STATEMENT & NUMERICAL APPROACH

The physical two-dimensional domain extends up to 600 km range in the main direction of the wind and 60 km altitude. The Earth's surface is modelled as a perfectly reflecting flat wall and the atmosphere as a vertically stratified medium. A Cartesian coordinate system Ox_1x_2 with origin at ground level is used. Sound propagation is governed by the two-dimensional Navier-Stokes equations including possible gravity effects [5]

$$\frac{\partial \mathbf{U}}{\partial t} + \frac{\partial \mathbf{E}_1}{\partial x_1} + \frac{\partial \mathbf{E}_2}{\partial x_2} - \frac{\partial \mathbf{V}_1}{\partial x_1} - \frac{\partial \mathbf{V}_2}{\partial x_2} + \frac{\partial \mathbf{Q}_1}{\partial x_1} + \frac{\partial \mathbf{Q}_2}{\partial x_2} + \mathbf{C} = \mathbf{\Lambda}_s \qquad \mathbf{U} = [\rho, \rho u_1, \rho u_2, \rho e_t]^T \tag{1}$$

The infrasonic source is placed at the origin of the domain and implemented as a forcing term in the energy equation, that is $\mathbf{\Lambda}_s = [0, 0, 0, \Lambda_s]$, with $\Lambda_s(x_1, x_2, t) = \mathcal{A}_s \sin(\omega_s t)[1 - \cos(\omega_s t)] \exp\left(-\log(2)(x_1^2 + x_2^2)/b_s^2\right)$ for $t \in [0, T_s]$. $\mathcal{A}_s$ is the amplitude, b_s the half-width and $f_s = \omega_s/(2\pi) = 1/T_s$ the frequency. In this work, b_s is set to 150 m and f_s to 0.4 Hz, so that the total emission duration is of $T_s = 2.5$ seconds. Finally, the amplitude is equal to $\mathcal{A}_s = 10^4$ J.m^{-3}.s^{-1} which gives an overpressure of about 100 Pa at 2 km from the source. The mean atmosphere, $\overline{\rho} = \overline{\rho}(x_2)$, $\overline{u}_1 = \overline{u}_1(x_2)$, $\overline{u}_2 \equiv 0$ and $\overline{\rho e_t} = \overline{\rho}(x_2)\overline{e_t}(x_2)$, is constructed from spline-based speed of sound $\overline{c}(x_2)$ and wind $\overline{u}_1(x_2)$ profiles, which reproduce the large scales observed during the Buncefield explosion. Data are extracted from ECMWF (European Centre for Medium-Range Weather Forecasts) profiles [6]. The atmospheric temperature $\overline{T}$ is computed according to the expression $\overline{T}(x_2) = \overline{c}(x_2)^2/(\gamma r)$, whereas the pressure profile $\overline{p}$ is obtained by solving the hydrostatic equilibrium equation $d\overline{p}/dx_2 = -g\overline{p}(r\overline{T})$. Finally, the density $\overline{\rho}$ is given by $\overline{\rho} = \overline{p}/(r\overline{T})$. Refer also to Marsden *et al.* [5] for further details on the present infrasound modelling.

System (1) is solved on a regular Cartesian grid with an optimized finite-difference time-domain algorithm [7, 8]. Spatial discretization is performed with an explicit fourth-order 11-point centered scheme. Time integration is carried out with a six-step second-order low-storage Runge-Kutta algorithm. An explicit fourth-order 11-point stencil spatial low-pass filter is applied to ensure stable computations. A shock-capturing procedure is employed to handle acoustic shocks which are generated during propagation [9]. Moreover, a moving domain technique is used to reduce the computing time and memory [10]. A regular grid with spacing $\Delta = \Delta x_1 = \Delta x_2 = 25$ m and a time step $\Delta t = 0.02$ s are adopted. The horizontal moving frame contains $7680 \times 2816 \sim 22$ million points and allows to cover a net range of 200 km. The numerical algorithm is implemented in the OpenCL environment and executed on a AMD Radeon R9 200 Series GPU (Graphics Processing Unit) with a memory allocation limit of 4 GB. The computation is carried out up to $t_{\max} = 2000$ s, requiring a total computational cost of about 24 hours.

RESULTS

The amplitude of the acoustic fluctuations is proportional to the square root of the local mean density [11]. The following normalized pressure variable is thus defined $\Phi = (p - \overline{p})/\sqrt{\overline{\rho}}$. Some snapshots of the field Φ are shown in Figure 2. Owing to the variations with height of the speed of sound and wind, acoustic waves are continuously refracted while propagating through the atmosphere. The wavefront released by the infrasonic source rapidly loses its initial cylindrical shape and a waveguide is generated between the Earths surface and about 40 km altitude, where the effective speed of sound, $\overline{c}_e = \overline{c} + \overline{u}_1$, becomes greater than its value at the ground. This waveguide effect is induced by the strong stratospheric wind. At $t = t_4 = 270.8$ s, a cusp caustic is observed, see also Figure 2. The acoustic rays which have reached the stratosphere turn now towards the Earth surface. The refracted wave consists of two wavefronts generated by the lower and higher stratospheric rays. They are clearly visible at $t = t_6 = 562.5$ s, where the upper arrival I_{sb1} precedes the lower one I_{sa1}.

The evolution of the acoustic signature along the x_2-axis is illustrated in Figures 3(a) and 3(b). Near the ground, at the point $B_1 = (0\,\text{km}, 2\,\text{km})$, the signal emitted by the infrasonic source exhibits a smooth sinusoidal shape with

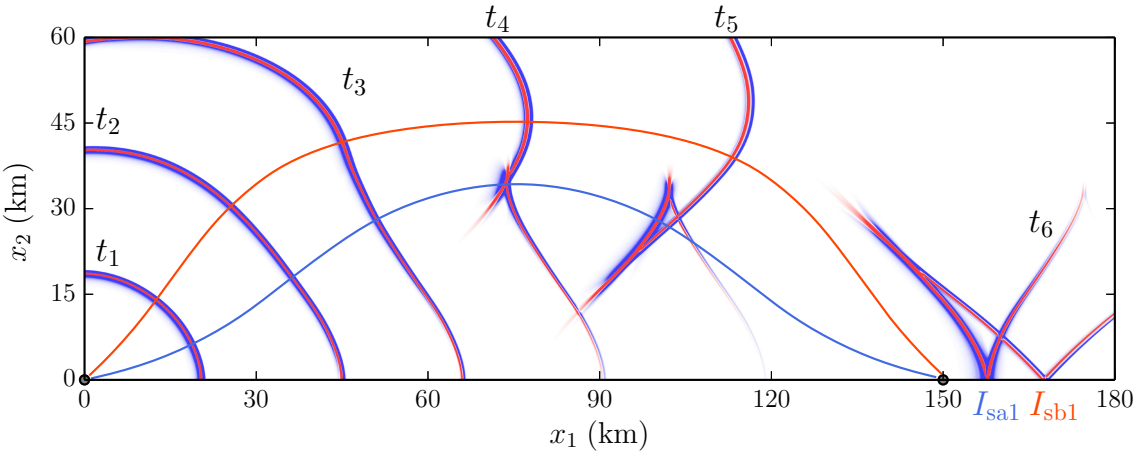

FIGURE 2. Snapshots of the overpressure Φ at different time instants (wavefronts t_1 to t_6)

a central frequency f_c around 0.34 Hz. At higher altitudes, as a consequence of the large amplitude and the reduction with height of the mean density, non-linearities become important and shocks are generated. At the point $B_2 = (0\,\text{km}, 60\,\text{km})$, an N-wave is observed, with a duration almost doubled.

The signal recorded at the ground station $S_1 = (150\,\text{km}, 0\,\text{km})$ is plotted in Figure 3(c). The two stratospheric arrivals I_{sa1} and I_{sb1} are well separated. In particular, the higher phase I_{sb1} is detected slightly earlier than the lower signal I_{sa1}, even though it propagates on a longer path (Figure 2). This effect is induced by the stratospheric wind speed, which is globally larger along the higher stratospheric rays. Finally, the lower arrival I_{sa1} exhibits the typical U-shaped waveform of an N-wave having passed through a caustic.

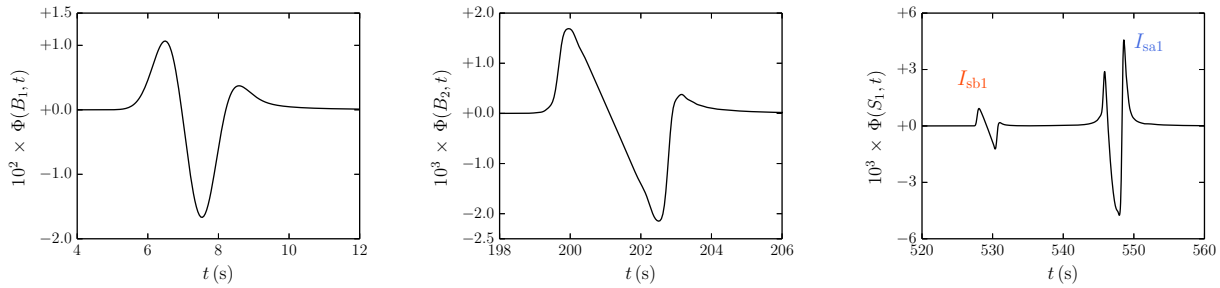

FIGURE 3. Overpressure Φ at $B_1 = (0\,\text{km}, 2\,\text{km})$ (a), at $B_2 = (0\,\text{km}, 60\,\text{km})$ (b) and at $S_1 = (150\,\text{km}, 0\,\text{km})$ (c).

The normalized pressure Φ recorded at ground level is illustrated in Figure 4(a) as a function of the distance from the source x_1 and the reduced time $t_r = t - x_1/\bar{c}(0\,\text{km})$. A tropospheric branch I_w is visible near the source. Its amplitude decay exponentially with x_1 [12]. The stratospheric pairs I_{sa}-I_{sb} are observed beyond the end of the first shadow zone, around 100 km range. Two pairs are recorded at the DIA ground station. The first arrival I_{sb2} is detected at a reduced time of about 100 s, corresponding to an apparent speed of 315 m.s^{-1}.

The signal at the DIA ground station is plotted in Figure 4 along with the recorded data. The numerical prediction on the travel times globally agrees with measurements. The largest misfits are found on the amplitude and waveforms of the different phases. Since the computation is performed in a two-dimensional frame, nonlinear effects are overestimated. More specifically, shock formation is anticipated in the initial vertical propagation. Consequently, the duration of the phases is lengthened and the signature modifications which occur at caustics are also affected. Moreover, it should be noted that the amplitude of the real source is not known and the value of 100 Pa used in this work is chosen in order for the propagation to remain in the weakly nonlinear regime.

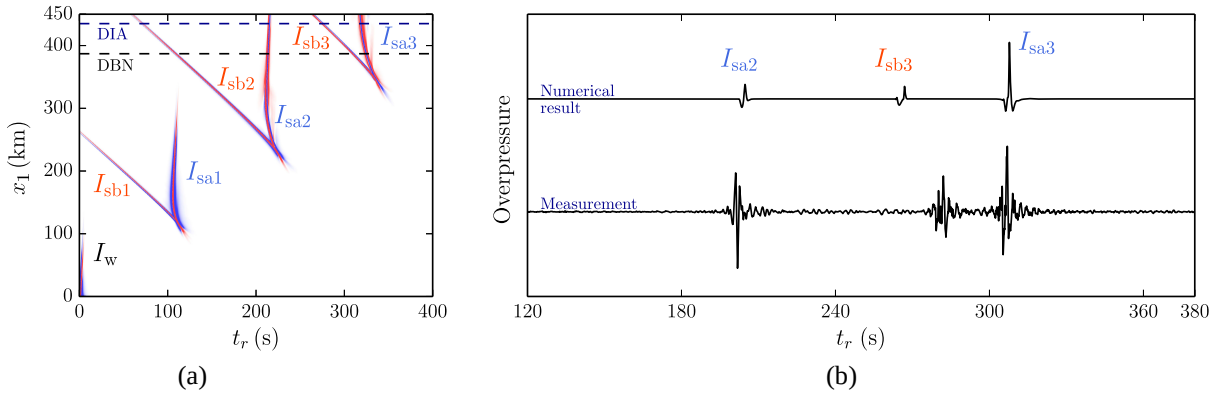

FIGURE 4. (a) Normalized pressure Φ as a function of range x_1 and of reduced time t_r. (b) Numerical prediction of the overpressure detected at the DIA ground station (upper signal) and recorded data.

CONCLUSION

The propagation of infrasonic signals in a realistic atmosphere and in the presence of a strong stratospheric wind is investigated in this work. A direct numerical simulation of the two-dimensional Navier-Stokes equations is performed to calculate the acoustic field. An optimized finite-difference time-domain method originally developed for aeroacoustic applications coupled with a moving frame technique is employed. Pairs of stratospheric arrivals are recorded at ground levels. At particular distances from the source, it is found that, in spite of a longer path length, the higher phase arrives earlier than the lower signal. All the physical phenomena involved in long-range infrasound propagation are included in the present modelling. This is however a first step towards three-dimensional simulations.

ACKNOWLEDGMENTS

Present results have been obtained within the frame of LETMA (Laboratoire ÉTudes et Modélisation Acoustique), Contractual Research Laboratory between CEA, CNRS, École Centrale de Lyon, C-Innov and Université Pierre et Marie Curie. This work was granted acces to the HPC resources of the Très Grand Centre de calcul du CEA (TGCC). The first author thanks the Direction Générale de l'Armement (DGA) for the financial support and the Labex CeLya of Université de Lyon.

REFERENCES

1. S.N. Kulichkov, I.P. Chunchuzov, G.A. Bush, and V.G. Perepelkin, Izvestiya, Atmospheric and Oceanic Physics, 44(2), 175–186 (2008).
2. L. Ceranna, A. Le Pichon, D. N. Green and P. Mialle, Geophys. J. Int. 117, 491–508 (2009)
3. L. G. Evers and H. W. Haak, Geophys. Res. Lett. 34, L10806 (2007)
4. L. Ottemöller and L. G. Evers, Geophys. J. Int. 172, 1123–1134 (2008)
5. O. Marsden, C. Bogey, and C. Bailly, J. Acoust. Soc. Am. 135(3), 1083-1095 (2014)
6. R. Waxler, L. G. Evers, J. Assink and P. Blom, J. Acoust. Soc. Am. 137(4), 1846–1856 (2015)
7. C. Bogey and C. Bailly, J. Comput. Phys., 194(1), 194–214 (2004)
8. J. Berland, C. Bogey, O. Marsden, and C. Bailly, J. Comput. Phys., 224, 637–662 (2007)
9. C. Bogey, N. De Cacqueray, and C. Bailly, J. Comput. Phys., 228, 1447–1465 (2008)
10. E. M. Salomons, R. Blumrich and D. Heimann, Acta Acust. united Ac. 88, 483–492 (2002)
11. P. G. Bergmann, J. Acoust. Soc. Am. 17(4), 329333 (1946)
12. A. D. Pierce, "Scattering and diffraction," in *Acoustics. An introduction to its physical principles and applications*, published by the Acoustical Society of America, New York, pp. 469–478.